ACS Catalysis

pubs.acs.org/acscatalysis
Research Article

Formaldehyde-Induced Deactivation of ZSM5 Catalysts during the Methanol-to-Hydrocarbons Conversion

Charles W. P. Pare, Przemyslaw Rzepka, Patrick Hemberger, Andras Bodi, Roland Hauert, Jeroen A. van Bokhoven,* and Vladimir Paunović*

Cite This: ACS Catal. 2024, 14, 463−474

ABSTRACT: Formaldehyde productivity and reactivity over zeolite catalysts are suggested to influence their selectivity and stability in the methanol-to-hydrocarbons (MTH) conversion. However, details of these relationships have yet to be established. In this study, we applied photoelectron photoion coincidence spectroscopy to examine the productivity of this intermediate over unpromoted and zinc-loaded ZSM-5 catalysts. Formaldehyde is the primary MTH product. Its production over unpromoted catalysts proceeds mainly via hydrogen transfer between methanol molecules, the rate of which is proportional to the concentration of strong Brønsted acid sites. In zinc-promoted ZSM-5, formaldehyde is mainly derived via methanol dehydrogenation, which provides up to a 12× higher productivity of this intermediate. The cumulative turnover capacity of the catalyst displays a strong negative correlation with its formaldehyde evolution activity. Formaldehyde evolution is enhanced at higher methanol concentrations and reaction temperatures, which are conditions also leading to enhanced coking. Complementary formaldehyde cofeeding experiments demonstrate that this intermediate enhances the formation of ethene and methylbenzenes over C_{3+} alkenes, which is in agreement with high selectivities to the products of the arene cycle over the catalysts with high formaldehyde productivity. The addition of formaldehyde promotes most substantially the deactivation of the most stable ZSM-5 catalysts displaying inherently low productivity of this intermediate, rendering their lifetimes comparable to those of their less stable counterparts. Operando diffuse-reflectance UV−vis spectra show that small amounts of formaldehyde greatly promote the conversion of cyclopentadienyl and methylated benzenyl intermediates into bicyclic and polycyclic aromatics. Consistent with this, formaldehyde cofeeding results in increased coke accumulation in more stable catalysts, especially in their micropores, as supported by X-ray diffraction and photoelectron spectroscopy analysis. These findings represent direct evidence that the stability and product distribution of ZSM-5 catalysts are strongly governed by their formaldehyde evolution activity.

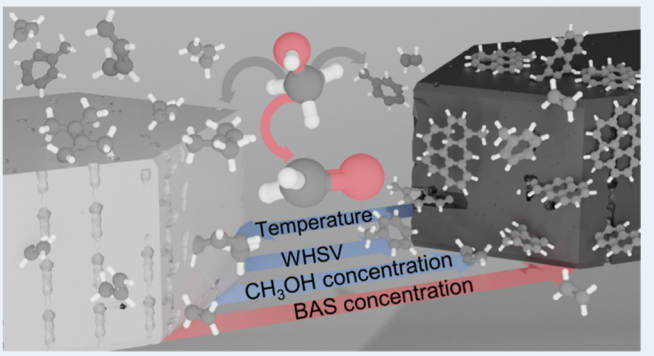

KEYWORDS: *methanol-to-hydrocarbons, formaldehyde, coking, deactivation, zeolites*

1. INTRODUCTION

The catalytic methanol-to-hydrocarbons (MTH) conversion process is an important pillar in retrofitting the existing infrastructure for petrochemical production to a range of fossil (e.g., coal and natural gas) and potentially renewable (e.g., carbon dioxide, hydrogen, and biomass) substitutes to crude oil because all of them can be readily converted into methanol.[1,2] MTH conversion is catalyzed by a range of molecular sieves, of which ZSM-5 zeolites and SAPO-34 zeotypes are industrially applied.[1−3] The micropore confinement along with Brønsted acid sites (BAS) in these materials allow the formation of alkene- and arene-based intermediates that act as cocatalysts in the synthesis of higher hydrocarbons.[1,2,4,5] In this so-called dual-cycle hydrocarbon pool (DCHP) mechanism, the alkene HP species undergo methylation and subsequent cracking reactions to produce C_{3+} alkenes, while analogous reaction sequences of the arene HP intermediates lead to the formation of ethene, propene, and arenes, including methylated benzenes and naphthalenes. Thereby, higher alkenes can be converted into arene intermediates via hydrogen transfer (HT) and cyclization reactions, in which alkanes are also produced.[5,6]

One of the critical limitations in the MTH conversion is the formation of higher-molecular-weight byproducts, mostly composed of polycyclic aromatic hydrocarbons (PAHs),

Received: September 10, 2023
Revised: November 26, 2023
Accepted: December 5, 2023
Published: December 21, 2023

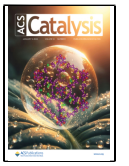

https://doi.org/10.1021/acscatal.3c04279
ACS Catal. 2024, 14, 463−474

which accumulate either on the outside of zeolite crystals or within their inner volume.[2,7−13] This creates the so-called external and internal coke deposits that occlude the active sites, thus causing a continuous loss of catalyst activity.[7,8,10,14] Consequently, MTH catalysts must be periodically regenerated by coke combustion at high temperatures (>823 K).[15] This procedure not only wastes up to ca. 8 mol % of methanol feed entrained in coke into carbon dioxide[16] but also causes a gradual decay of the catalyst due to the high temperatures applied and prominent steam evolution.[17−19]

The catalyst's propensity to deactivate is strongly dependent on its structure and operating regime. Medium-pore molecular sieves are most stable, while small-pore sieves are least stable, with large-pore systems exhibiting intermediate stability.[1,2,4] The catalyst stability increases with decreasing crystallite size and BAS density.[20−25] Besides, specific extraframework cations (e.g., zinc) can increase, while others (e.g., calcium) can decrease the catalyst's propensity to coking.[25−29] Regarding process parameters, coke-induced deactivation is enhanced at high temperatures,[8,30] methanol concentrations,[8,31] and weight hourly space velocities (WHSVs).[32,33]

Coke species are regarded as byproducts of DCHP reactions, originating from excessive methylation of coke precursors, primarily arenes.[2,4,8,13] It is commonly accepted that the formation of PAHs proceeds primarily through the alkene-induced HT (AIHT) reactions, which comprises protonation of (cyclo)alkene, followed by a hydride transfer from another (cyclo)alkene to thus obtained surface-bound alkyl species.[6,13] AIHT thus results in the formation of (cyclo)alkanes and unsaturated (cyclo)dienes, which are readily converted into arenes. However, recent studies pointed out that coke-forming reactions and the product distribution in the MTH reaction are strongly influenced by formaldehyde.[8,9,31,34−41] This reactive intermediate is derived via methanol-induced HT (MIHT), in which methanol or DME is the hydride donor.[6,37,39,42−46] The acceptor can either be a surface methyl species generated by adsorption of methanol or DME, or a surface alkyl species stemming from adsorption of an unsaturated hydrocarbon, typically an alkene, on an acid site. Along with formaldehyde, these so-called MIHT reactions produce methane and water, and more saturated hydrocarbons (e.g., alkanes). Recently, we showed that formaldehyde can also arise from methanol dehydrogenation over transition metal sites that may be present in the reactor walls and the bed-diluents.[47] Formaldehyde is proposed to react with alkenes via Prins and hydroacylation reactions yielding dienes and polyenes, which readily undergo cyclization and HT, eventually yielding arenes.[6,11,37,40,43,48,49] Besides, formaldehyde can directly convert arenes into deactivating species, such as diphenylmethane.[40] These formaldehyde-mediated reactions (FMRs) are catalyzed by BAS,[37,43] and can be additionally promoted by Lewis acid sites (LAS).[6] They are also suspected to be the central promotors of the arene cycle and associated pathways that cause the formation of coke.[6,37,43,44] However, the contribution of the FMRs to the deactivation of the catalysts exhibiting different acid properties under different reaction conditions is still elusive. This is to a significant extent caused by the challenging detection of this intermediate by conventional mass spectrometry and gas-chromatography techniques.[38,47]

Herein, we applied a multitechnique approach to evaluate the long-debated relationships between the product distribution, propensity to coking, and the formaldehyde-evolution activity using a series of practically relevant ZSM-5 catalysts. In particular, we assessed the inherent productivity of formaldehyde over a series of ZSM-5 catalysts by utilizing photoelectron photoion coincidence (PEPICO) spectroscopy, which was demonstrated previously as a highly sensitive technique to analyze the formation of this intermediate over zeolite and nonzeolite based materials.[38,47,50] We also applied operando diffuse reflectance UV−vis (DR/UV−vis) spectroscopy to assess the evolution of active and deactivating intermediates over these materials in the absence and presence of the formaldehyde cofeeds.[51−53] Complemented with the analysis of the impact of the formaldehyde cofeeds on the catalyst lifetime, selectivity, and coking of zeolite, our results unveil an important role of formaldehyde in controlling the zeolite stability in the MTH conversion.

2. EXPERIMENTAL SECTION

2.1. Catalysts and Characterization. Commercially available ZSM-5 zeolites with nominal Si/Al ratios of 15 (Zeolyst, CBV 3024E), 25 (Zeolyst, CBV 5524G), 40 (Zeolyst, CBV 8014), and 140 (Zeolyst, CBV 28014) were received in ammonium form and converted into the proton form by calcination. The resulting catalysts are termed Z_{15}, Z_{25}, Z_{40}, and Z_{140}, respectively. A zinc-exchanged Z_{40} zeolite, coded ZnZ_{40}, was synthesized by incipient wetness impregnation of Z_{40} (ammonium form) with an aqueous solutions of zinc acetate dihydrate ($Zn(CH_3COO)_2{\cdot}2H_2O$, Merck, >99%) to attain a nominal loading of zinc of 1.0 wt %, followed by drying under vacuum (100 mbar) at 373 K for 12 h. All catalysts were calcined under an oxygen flow (Pangas, 5.0, F_{O_2} = 100 cm_{STP}^3 min^{-1}) at 823 K for 5 h with a heating rate of 2 K min^{-1}. Fresh catalysts were characterized by nitrogen adsorption, powder X-ray diffraction, and pyridine adsorption using Fourier-transform infrared (FTIR) spectroscopy, while the coke content and distribution in deactivated catalysts were probed by thermogravimetric (TGA) analysis and X-ray photoelectron spectroscopy (XPS). These characterization methods are detailed in the Supporting Information.

2.2. Catalytic Testing. The MTH conversion reactions were carried out in an automated homemade continuous-flow fixed-bed reactor setup. Unless otherwise stated, the reaction was conducted at 673 K and total pressure of P = 1.5 bar using an argon flow of F_{Ar} = 190 cm_{STP}^3 min^{-1} with a methanol flow of F_{CH_3OH} = 0.04 cm_{lq}^3 min^{-1}, which corresponds to a methanol concentration of c_{CH_3OH} = 11 mol % in the feed. In the formaldehyde cofeeding experiments, formaldehyde was added in the concentration of c_{CH_2O} = 0.5, 1, or 2 mol_C % (mol_C % stands for fraction of component in total carbon content). Details on reactor setup, catalytic testing, calculation of conversion, product selectivities, and cumulative turnover-capacities are provided in the Supporting Information.

2.3. PEPICO and *Operando* DR/UV−Vis Spectroscopy Experiments. Photoelectron photoion coincidence (PEPICO) spectroscopy analysis of formaldehyde and other products in the MTH reaction outlet was performed at the vacuum ultraviolet (VUV) beamline of the Swiss Light Source (Figure S1)[54−57] using a similar approach as described in our previous work.[47] Unless otherwise stated, the MTH reaction was conducted using c_{CH_3OH} = 1.95 mol %, $WHSV$ = 1.3−10.9 g_{CH_3OH} g_{cat}^{-1} h^{-1}, T = 548−698 K, and P = 0.4 bar. *Operando* diffuse-reflectance UV−visible (DR/UV−vis) spectroscopy

https://doi.org/10.1021/acscatal.3c04279
ACS Catal. 2024, 14, 463−474

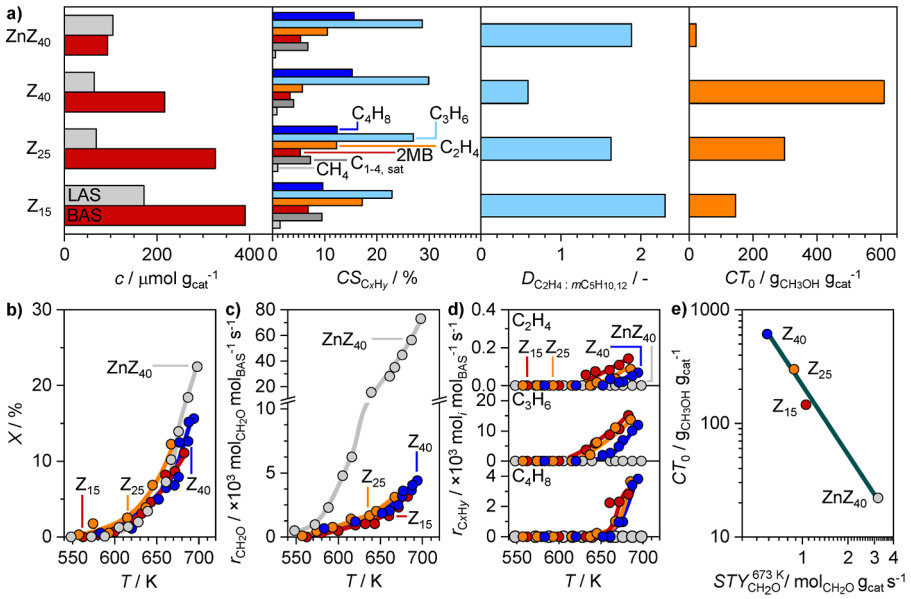

Figure 1. (a) Concentration of strong BAS and LAS in different ZSM-5 zeolites, cumulative selectivities to specific products ($CS_{C_xH_y}$), ethene-to-2-methylbutane/butene selectivity ratios ($D_{C_2H_4/mC_5H_{10,12}}$), and cumulative turnover capacities (CT_0) measured in MTH catalytic tests. The values of $CS_{C_xH_y}$ and $D_{C_2H_4/mC_5H_{10,12}}$ were determined in the conversion range of ca. 30−50% from the selectivity−conversion profiles shown in Figure S3. (b) Methanol conversion and apparent evolution rates of (c) formaldehyde and (d) light alkenes *versus* temperature in the MTH reaction over different ZSM-5 catalysts determined by PEPICO experiments. (e) The relationship between the CT_0 measured in the MTH catalytic tests and the space-time yields of formaldehyde determined by the PEPICO experiments at 673 K. Conditions in the MTH catalytic tests: *WHSV* = 38 (Z_{40}, ZnZ_{40}), 44 (Z_{25}), or 51 $g_{CH_3OH}\ g_{cat}^{-1}\ h^{-1}$, c_{CH_3OH} = 11 mol %, T = 673 K, and P = 1.5 bar. Conditions in the PEPICO experiments: *WHSV* = 4.4 (Z_{40}, ZnZ_{40}), 6.0 (Z_{25}), or 10.9 $g_{CH_3OH}\ g_{cat}^{-1}\ h^{-1}$ (Z_{15}), c_{CH_3OH} = 1.95 mol %, T = 673 K, and P = 0.4 bar.

analysis of the reaction intermediates retained by the zeolite catalysts was performed in a home-built cell closed with a calcium fluoride window (Figure S1). The MTH catalytic tests were performed using a feed of c_{CH_3OH} = 11 mol %, c_{CH_2OH} = 0 or 2 mol_C %, *WHSV* = 33−60 $g_{CH_3OH}\ g_{cat}^{-1}\ h^{-1}$, T = 673 K, and P = 1.2 bar. Details on the PEPICO and DR/UV−vis reactor setups and the reaction analysis are provided in the Supporting Information.

3. RESULTS AND DISCUSSION

3.1. MTH Performance−Formaldehyde Formation Relationships. It is well-established that the acidity of the ZSM-5 catalysts, which is primarily determined by their Si/Al ratios and by the presence of the extraframework cations, has a strong impact on their activity, selectivity, and stability in the MTH reaction.[21,23,25] Catalysts with low BAS concentration are more selective toward C_{3+} alkenes and display a lower propensity to coking. This is typically ascribed to less prominent HT reactions, including methanol HT leading to formaldehyde.[6] However, the details of the relationship between catalyst acidity, formaldehyde evolution and reactivity, and the MTH performance remain elusive.

We commenced analyzing these relationships by evaluating the ZSM-5 catalysts with Si/Al ratios of 15, 25, and 40, and a zinc-promoted catalyst with a Si/Al ratio of 40. The concentration of strong BAS in these materials decreased in the order of Z_{15} (391 $\mu mol\ g^{-1}$) > Z_{25} (326 $\mu mol\ g^{-1}$) > Z_{40} (217 $\mu mol\ g^{-1}$) > ZnZ_{40} (93 $\mu mol\ g^{-1}$), while the strong LAS concentration displayed the following trend: Z_{15} (172 $\mu mol\ g^{-1}$) > ZnZ_{40} (105 $\mu mol\ g^{-1}$) > Z_{25} (64 $\mu mol\ g^{-1}$) ≈ Z_{40} (60 $\mu mol\ g^{-1}$, Figures 1a, S2 and Table S1). The unpromoted catalysts with higher BAS concentration displayed lower selectivities to propene and butene and higher selectivities to ethene and 2-methylbenzene (2MB), indicating the prevalence of the arene over alkene-mediated reactions in BAS-rich materials (Figure 1a). This is also reflected in a higher ethene-to-2-methylbutane/butene selectivity ratio ($D_{C_2H_4/mC_5H_{10,12}}$) over the catalysts with an increased BAS concentration, which is a descriptor for the relative prevalence of the arene over the alkene cycle.[31] In agreement with the prominent role of arene chain carriers in initiating coke-forming reactions, the catalyst stability measured as a cumulative turnover capacity (CT_0) decreased in the order: Z_{40} (610 $g_{CH_3OH}\ g_{cat}^{-1}$) > Z_{25} (300 $g_{CH_3OH}\ g_{cat}^{-1}$) > Z_{15} (145 $g_{CH_3OH}\ g_{cat}^{-1}$, Figure 1a). However, the ZnZ_{40} catalyst displayed a clear deviation from the aforementioned BAS-based trend. Although exhibiting a ca. 2.3× lower BAS concentration than the parent Z_{40} zeolite, it showed unchanged selectivities to propene and butene, and increased selectivities to ethene (ca. 1.8×) and 2MB (ca. 1.6×) with respect to the parent Z_{40} catalyst. Moreover, the $D_{C_2H_4/mC_5H_{10,12}}$ ratio in ZnZ_{40} (ca. 1.9) is comparable to those of BAS-rich Z_{25} (ca. 1.6) and Z_{15} (ca. 2.3) catalysts, while its CT_0 value (22 $g_{CH_3OH}\ g_{cat}^{-1}$) is drastically lower than that of the latter zeolites (Figure 1a).

The selectivity and stability differences between the ZSM-5 materials correlate with their different activities in HT reactions. This can be inferred from the increasing selectivities to methane and C_{1-4} alkanes over Z_{40}, Z_{25}, and Z_{15} catalyst series and substantially higher (ca. 1.7×) selectivity to C_{1-4} in ZnZ_{40} than in Z_{40} (Figure 1a). Since these catalysts were evaluated at initial methanol conversions of $X_{initial}$ ≈ 70−90% for unpromoted catalysts and $X_{initial}$ ≈ 50% for ZnZ_{40} (Figure S3), MIHT reactions are suspected to dominate HT.[6] As a

https://doi.org/10.1021/acscatal.3c04279
ACS Catal. 2024, 14, 463−474

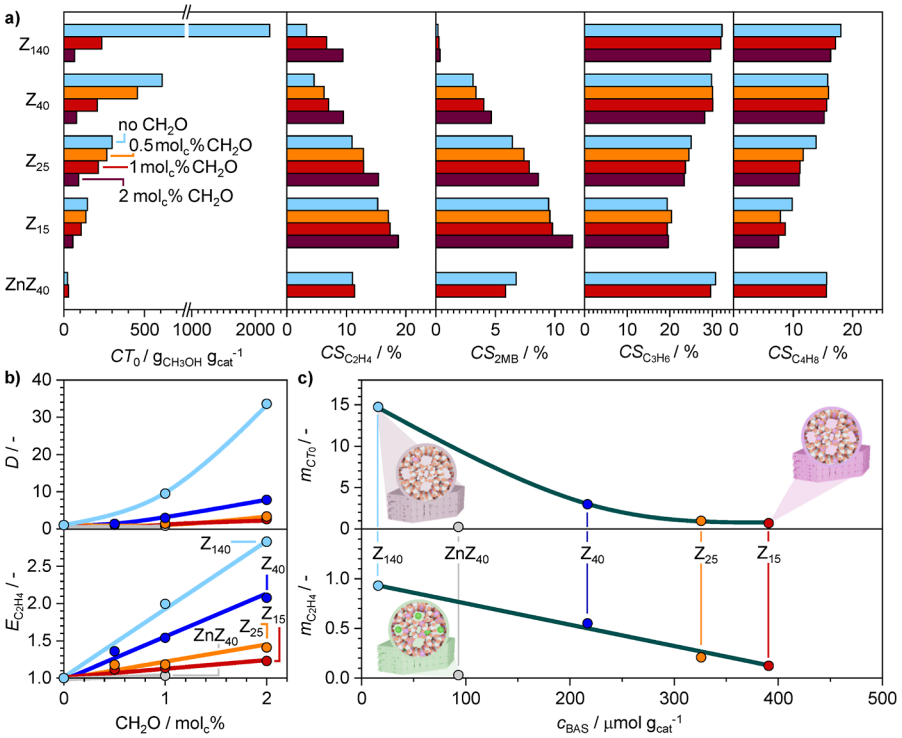

Figure 2. (a) Cumulative turnover capacities (CT_0), and cumulative selectivities to ethene ($CS_{C_2H_4}$), 2MB (CS_{2MB}), propene ($CS_{C_3H_6}$), and butene ($CS_{C_4H_8}$) in the MTH reaction over ZSM-5 zeolites in the absence and in the presence of formaldehyde cofeeds. (b) Relative change of cumulative turnover (D) and selectivity to ethene ($E_{C_2H_4}$) sensitivity factors *versus* cofeed concentration of formaldehyde in MTH over ZSM-5 zeolites. (c) Dependency of cumulative turnover (m_{CT_0}) and ethene ($m_{C_2H_4}$) sensitivity factors to formaldehyde cofeeding over ZSM-5 catalysts with different acid properties. Symbols represent the experimental data, and lines are intended to guide the eye. Conditions: *WHSV* = 13 (Z_{140}), 38 (Z_{40}, ZnZ_{40}), 44 (Z_{25}), or 51 $g_{CH_3OH}\ g_{cat}^{-1}\ h^{-1}$, c_{CH_3OH} = 11 mol %, c_{CH_2O} = 0, 0.5, 1, or 2 mol_C %, T = 673 K, and P = 1.5 bar.

result, catalysts with higher MIHT activity are expected to generate a higher amount of formaldehyde, which may induce a series of FMRs that promote coking.[9,31,34,37]

To inspect the role of the MIHT reactions, the formaldehyde productivity over the aforementioned ZSM-5 catalyst series was assessed by PEPICO spectroscopy. The catalysts activities were evaluated at reduced pressures and increased *WHSV*s. *WHSV*s were adjusted to attain low and comparable conversion levels over the catalysts (≤16% for unpromoted zeolites, ≤32% for ZnZ_{40}) in the temperature range of 548−698 K, which captures the typical operating window of the MTH reaction (Figure 1b). In this reaction regime, formaldehyde was detected over all catalysts (Figures 1c and S4 and Table S2). The "wall-catalyzed" formation of formaldehyde was greatly minimized by the use of a quartz reactor and quartz bed diluent (Figure S4).[47] The evolution of formaldehyde over Z_{15}, Z_{25}, and Z_{40} catalysts was accompanied by the formation of methane and subsequently ethene, propene, and butene (Figures 1d and S5). The onset of light alkene production shifted to ca. 30 K higher temperatures than that of formaldehyde production, corroborating the assumption that formaldehyde, along with methane (Figure S5), is the first gaseous intermediate generated in the MTH reaction. Alkanes, such as propane and butane, were not detected in the outlet reactor stream, which points toward MIHT in which methanol or DME are hydrogen acceptors as the primary source of formaldehyde. Moreover, the increasing production of formaldehyde with rising temperature along with virtually nondetectable formation of arenes, such as benzene and methylbenzene (MB), and dienes, such as butadiene (Figure S5), indicates that the consumption of this reaction intermediate through subsequent reactions with alkene or arene chain carriers is greatly suppressed. Therefore, the measured formaldehyde evolution rates are representative of the inherent formaldehyde productivity over that of the respective catalyst. Notably, the formaldehyde formation rates over unpromoted ZSM-5 zeolites normalized per their strong BAS concentration are almost indistinguishable (Figure 1c). This is a strong indication that strong BAS are the main active sites responsible for formaldehyde formation over these materials. In good agreement with the performance differences observed in the laboratory fixed-bed reactor tests, the ZnZ_{40} catalyst displayed substantially higher (ca. 7−12×) formaldehyde formation rate per BAS. The nondetectable formation of methane and other hydrocarbons, and detection of hydrogen over ZnZ_{40}, which is not observed over unpromoted zeolites, suggests that the extraframework zinc cations introduce another, highly reactive pathway of formaldehyde formation via methanol dehydrogenation (Figure S5). Because of its low BAS concentration and high formaldehyde evolution activity, ZnZ_{40} is thus an interesting catalytic material for assessing the impact of formaldehyde on catalyst stability.

We can now compare the formaldehyde space-time yields (STY_{CH_2O}) under conditions that minimize its consumption by sequential reactions with CT_0. Notably, CT_0 displays a strong negative correlation with STY_{CH_2O}, which is calculated as the product of the strong BAS concentration and the formaldehyde

https://doi.org/10.1021/acscatal.3c04279
ACS Catal. 2024, 14, 463−474

formation rate per strong BAS concentration of a given catalyst in the PEPICO experiments performed at the same temperature (673 K, Figure 1e and eq S7). This provides a hint that formaldehyde, which is generated as the primary intermediate in the MTH conversion, has a considerable impact on the reaction cascades, leading to catalyst coking and consequent deactivation.

3.2. Impact of Formaldehyde Formation on the Catalyst Stability. To reveal further relationships between catalyst acidity, FMR activities, and stability, as implied by a strongly negative CT_0−STY_{CH_2O} correlation (Figure 1e), the impact of formaldehyde cofeeding (0.5−2 mol_C %) on the MTH performance was studied. As formaldehyde is produced in the first sections of the catalyst bed (Figure 1b,c), cofeeding of small concentrations of this MTH product (0.5−2 mol_C %) that are comparable to its yield determined by PEPICO experiments (Figure S4), closely emulates its enhanced formation. In this way, they enable us to assess the deactivation potential of this intermediate, which is especially relevant for catalysts with low BAS concentration. The impact of formaldehyde cofeeds was studied over the previously discussed set of ZSM-5-based catalysts enriched by a low-acidic Z_{140} zeolite (strong c_{BAS} = 16 μmol g^{-1}). Z_{140} displays a very stable MTH performance with high selectivities to propene and butene, and low selectivities to ethene and 2MB (Figures 2a and S3). The addition of formaldehyde led to a decrease in the CT_0 values and an increase in the cumulative selectivities to ethene and arenes over all unpromoted zeolites. However, the magnitude of these changes increases strongly with decreasing BAS concentration. Specifically, the addition of 2 mol_C % formaldehyde to the methanol feed decreased CT_0 by ca. 3× for Z_{15}, and by ca. 34× over the Z_{140} catalyst. The addition of 2 mol_C % formaldehyde to the methanol feed over Z_{140} decreased its CT_0 from 2220 g_{CH_3OH} g_{cat}^{-1} to only 78 g_{CH_3OH} g_{cat}^{-1}, which is significantly lower than that of the highly acidic Z_{15} material (145 g_{CH_3OH} g_{cat}^{-1}, Figure 2a). The formaldehyde cofeeds also affected the product distribution. More specifically, the selectivity to ethene and 2MB progressively increased, while the butene selectivity decreased, corroborating the promotion of the arene cycle by the formaldehyde intermediate. Similar to the stability, the relative changes in the ethene selectivity were more pronounced over Z_{140} (ca. 2.8×) than over Z_{15} (ca. 1.2×) catalyst (Figures 2a and S3). In contrast, the inherently low CT_0 values and product distribution of ZnZ_{40} material were virtually unaffected by the formaldehyde cofeed (Figures 2a and S3).

More quantitative insights into the impact of the formaldehyde cofeeds on the MTH performance can be obtained by evaluating the relative sensitivity factors for CT_0 and cumulative product selectivity (Figure 2b). The deactivation factor (D) is defined as the ratio between the cumulative turnover capacities in the absence ($CT_{0,M}$) and in the presence (CT_{0,fCH_2O}) of the formaldehyde cofeed. Under the premises of a simplified reaction model, which assumes that (1) the catalyst deactivates nonselectively, (2) the deactivation rate follows a first-order dependence with respect to active sites and deactivating species, (3) the deactivation involves formaldehyde-independent and formaldehyde-dependent pathways, and (4) the latter pathways follow the pseudo-first-order dependence with respect to formaldehyde, the dependence of factor D on the concentration of cofed formaldehyde ($[CH_2O]_{co}$) is dependent on the inherent formaldehyde productivity ($[CH_2O]_{inh}$) according to eq 1 (Supporting Information Discussion S2.1 provides derivation details). Herein, R_D reflects the ratio between formaldehyde-independent and formaldehyde-dependent deactivation.

$$D = \frac{CT_{0,M}}{CT_{0,fCH_2O}} = 1 + \frac{1}{R_D + [CH_2O]_{inh}}[CH_2O]_{co} = 1 + m_{CT_0}[CH_2O]_{co} \quad (1)$$

Hence, the catalyst exhibiting lower inherent productivity of CH_2O under specific conditions is expected to display a larger change in D upon cofeeding formaldehyde. The prominent changes of D induced by miniscule amounts of formaldehyde in the cofeed indicate that even small differences in inherent productivity of formaldehyde have a strong impact on the catalyst performance. Such effects further suggest that the parameter R_D is relatively low in the experiments performed in this work and that changes in the sensitivity factors are primarily determined by the inherent productivities of formaldehyde.

In analogy to factor D, the product selectivity change factor, $E_{C_xH_y}$, can be defined as the ratio between the cumulative selectivities to product C_xH_y, in the presence, $CS_{C_xH_y,fCH_2O}$, and in the absence, $CS_{C_xH_y,M}$, of formaldehyde cofeed. Under the assumption that formation of products proceeds via the acid-site catalyzed reactions of an oxygenate (methanol or DME) with formaldehyde-dependent or the formaldehyde-independent fractions, the dependence of $E_{C_xH_y}$ on the concentration of the cofed formaldehyde ($[CH_2O]_{co}$) is a function of the concentration of the inherently formed formaldehyde ($[CH_2O]_{inh}$) and the ratio between the formaldehyde-independent and formaldehyde-dependent product formation ($L_{C_xH_y}$) and the formaldehyde dependency factor ($b_{C_xH_y}$, eq 2, Supporting Information Discussion S2.2 for derivation details).

$$E_{C_xH_y,fCH_2O} = \frac{CS_{C_xH_y,fCH_2O}}{CS_{C_xH_y,M}} = 1 + b_{C_xH_y}\frac{1}{L_{C_xH_y} + [CH_2O]_{inh}}\cdot[CH_2O]_{co} = 1 + m_{C_xH_y}[CH_2O]_{co} \quad (2)$$

As discussed above, the impact of formaldehyde on product formation can be positive, negative, or negligible. For example, $E_{C_2H_4}$ displays a strong positive and $E_{C_4H_8}$ a strong negative dependency on the concentration of cofed formaldehyde (Figures 2b and S6). These products stem from arene and alkene cycles, respectively. Such changes in selectivity reflect the formaldehyde-induced conversion of alkenes into arene chain carriers. The absence of substantial $E_{C_3H_6}$ variance with introducing formaldehyde in the feed suggests that the productivity of propene by the arene cycle compensates for the losses caused by decreasing alkene cycle (Figures S3 and S6).

Based on the previously described models, the slopes of factor D and $E_{C_xH_y}$ dependences on the concentration of cofed

https://doi.org/10.1021/acscatal.3c04279
ACS Catal. 2024, 14, 463−474

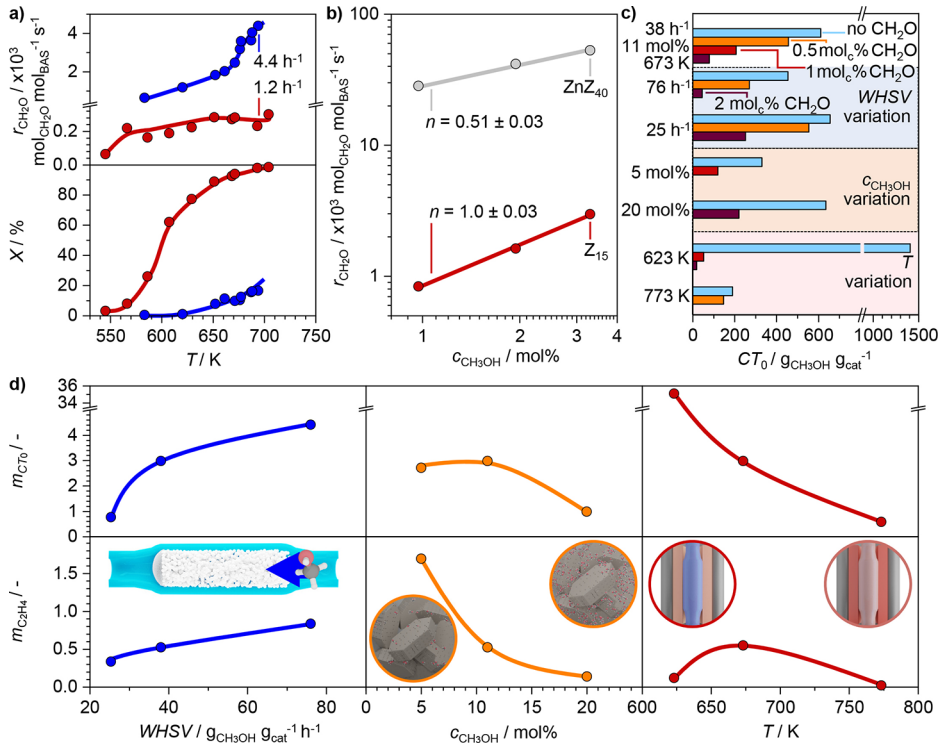

Figure 3. (a) Apparent evolution rates of formaldehyde (top) and methanol conversion (bottom) *versus* temperature in the MTH reaction over Z_{40} at two *WHSV*s. (b) Apparent evolution rates of formaldehyde *versus* inlet methanol concentration in the MTH reaction over ZnZ_{40} and Z_{15} at 673 and 637 K, respectively. Data in (a,b) are determined by the PEPICO experiments. (c) Cumulative turnover capacities (CT_0) in the MTH reaction over Z_{40} zeolite in the absence and in the presence of formaldehyde cofeeds at different *WHSV*s, inlet methanol concentrations, and temperatures, which are indicated on the vertical axis. Top data set represents the performance under the benchmark conditions. (d) Cumulative turnover (m_{CT_0}, top) and ethene ($m_{C_2H_4}$, bottom) sensitivity factors over Z_{40} *versus WHSV*s (left), methanol concentration (middle), and temperature (right). Symbols represent the experimental data; continuous lines are intended to guide the eye. Except for *WHSV*s, other conditions of the PEPICO experiments correspond to those reported in the caption of Figure 1. Benchmark conditions in the MTH catalytic tests unless otherwise indicated in the plot: *WHSV* = 38 g_{CH_3OH} g_{cat}^{-1} h^{-1}, c_{CH_3OH} = 11 mol %, c_{CH_2O} = 0, 0.5, 1, or 2 mol_C %, T = 673 K, and P = 1.5 bar.

formaldehyde, m_{CT_0} and $m_{C_xH_y}$, respectively, provide information on the inherent formaldehyde productivity (eqs 1 and 2, Figures 2b and S6). Both m_{CT_0} and $m_{C_2H_4}$ display a strong negative correlation with the concentration of BAS over unpromoted catalysts, and are virtually equal to zero for the ZnZ_{40} (Figure 2c). Such a behavior agrees with the experimentally measured order of catalyst activities in the formaldehyde formation reactions (Figure 1e), demonstrating the validity of the simplified reaction model. The exceptional behavior of ZnZ_{40} is in agreement with a high formaldehyde productivity induced by the introduction of zinc.[26,28] Therefore, cofeeding formaldehyde to this reactive system has virtually no impact on its performance. Overall, cofeeding experiments further evidence that a relatively small increase in the formaldehyde formation can greatly promote the formation of products arising from the arene cycle and coke-forming reactions. Therefore, the lower productivity of formaldehyde over the less acidic zeolites can be the source to their higher selectivity toward the products of the alkene cycle and their lower propensity to coking.

3.3. Impact of Reaction Conditions. Formaldehyde is a primary intermediate in MTH conversion, which is proposed to readily react within the reaction network. The PEPICO analysis of the formaldehyde evolution over Z_{40} catalyst at two *WHSV*s that result in a low and high methanol conversion supports this proposal (Figure 3a). More specifically, the increase of temperature in a low *WHSV* experiment (1.2 h^{-1}) leads to a prominent rise of the formaldehyde productivity up to conversions of ca. 20%. However, the apparent formaldehyde production displays a small increment in the conversion range of up to ca. 80%, and is virtually constant at near complete reactant consumption. Notably, the effective productivities of formaldehyde measured at low *WHSV* and high conversions are ca. 5−18× lower than those measured at increased *WHSV* and decreased conversions in the same temperature range. This result demonstrates that formaldehyde is promptly consumed upon establishment of the DCHP reaction network at moderate and high conversion levels.

The inlet methanol concentration also affects formaldehyde productivity.[8,31] The analysis performed at increased *WHSV*s over Z_{15} and ZnZ_{40} zeolites, which are representative of the two distinct activity patterns in formaldehyde evolution, demonstrates a positive reaction order of formaldehyde formation with respect to the inlet methanol concentration (Figure 3b). However, while the reaction displays an apparent reaction order of ca. 1 over the Z_{15} catalyst, the apparent reaction order is ca. 0.5 in the case of ZnZ_{40}. The former reaction order is consistent with the BAS-catalyzed MIHT mechanism in which the HT between surface-bound methyl group and methanol is likely the rate-limiting step (see Supporting Information Discussion S2.3 for derivation).[43] On the other side, the reaction order measured over ZnZ_{40} can be rationalized by the previously proposed dehydrogenation

https://doi.org/10.1021/acscatal.3c04279
ACS Catal. 2024, 14, 463−474

mechanism, in which the dehydrogenation of methanol is the likely rate-determining step (please see Supporting Information Discussion S2.3 for derivation details).

The productivity and reactivity of formaldehyde can also be studied by assessing the CT_0 and the product distribution of the archetypical Z_{40} catalyst at different *WHSV*s and methanol concentrations in the absence and in the presence of formaldehyde cofeeds (0−2 mol_C %, Figures 3c and S7).[37,38,47] We studied MTH performance at 673 K and *WHSV*s of 76, 38, and 25 $g_{CH_3OH}\ g_{cat}^{-1}\ h^{-1}$, which resulted in low (ca. 40%), medium (ca. 77%), and complete (ca. 100%) initial conversions (Figure S7), respectively. Consistent with the nonselective deactivation model of ZSM-5 catalysts, the selectivity−conversion profiles recorded during deactivation are virtually independent of the initial activity (Figure S7). The selectivities to the products of the arene HP (e.g., ethene and 2MB) and light alkanes decreased, while the selectivities to the products of the alkene HP (e.g., butene) and propene increased with increasing conversion. In agreement with previous work,[32] CT_0 increases with the decrease of the *WHSV* from 76 to 25 $g_{CH_3OH}\ g_{cat}^{-1}\ h^{-1}$. These changes in the catalytic performance were previously associated with the increase of the average methanol concentration per active site at higher *WHSV*, which is proposed to enhance formaldehyde evolution via methanol-induced HT, and thus the formation of the arene HP and coke.[32]

The addition of formaldehyde had a marginal effect on the initial conversion in all *WHSV*s. However, the relative increase of selectivity toward the products associated with the arene cycle and the reduction of the CT_0 values were much more pronounced in the experiment performed at higher than at lower *WHSV* (Figures 3c and S7). More specifically, at a low *WHSV* of 25 $g_{CH_3OH}\ g_{cat}^{-1}\ h^{-1}$, the addition of 2 mol_C % formaldehyde decreased the CT_0 and increased ethene cumulative selectivity by 2.6× and 1.7×, respectively, whereas at a high *WHSV* of 76 $g_{CH_3OH}\ g_{cat}^{-1}\ h^{-1}$, CT_0 decreased 10× and ethene selectivity increased 2.7× (Figures 3c and S8). Such enhanced sensitivity of D and $E_{C_2H_4}$ at higher *WHSV*s, as indicated by the m_{CT_0} and $m_{C_2H_4}$ slopes (Figures 3d and S8), is consistent with previously observed higher sensitivity of ZSM-5 catalysts with lower BAS concentration (Figure 2c), as each single BAS experiences a higher effective formaldehyde concentration in both cases. Since the CT_0 value of the whole catalyst bed represents the average of the CT_0 values of its various sections (Supporting Information Discussion S2.4), these catalytic data demonstrate that an increase of the formaldehyde concentration in the inlet feed (from 0 to 2 mol_C %) leads to a much more pronounced CT_0 drop in the first bed section (from ca. 450 to ca. 45 $g_{CH_3OH}\ g_{cat}^{-1}$) when compared to the last bed section (from ca. 750 to ca. 600 $g_{CH_3OH}\ g_{cat}^{-1}$). These results corroborate the PEPICO measurements of the formaldehyde productivity, which show that formaldehyde evolution and its subsequent conversion into coke precursors occur in the first sections of the catalyst bed, corresponding to the moderate conversion levels of ca. 20−30%.

Analogously, MTH was performed over Z_{40} at three different methanol concentrations (5, 11, and 20 mol %) and a constant *WHSV* of 38 $g_{CH_3OH}\ g_{cat}^{-1}\ h^{-1}$ (Figure S9) to investigate the influence of methanol concentration on the formaldehyde sensitivity. The increase of the inlet methanol concentration from 5 to 20 mol % led to an increase of the initial conversion from 40% to almost 100%, in agreement with the positive reaction order of methanol in MTH.[58] CT_0 values also increase (from 300 to 635 $g_{CH_3OH}\ g_{cat}^{-1}$). This can be rationalized by a steeper gradient of methanol concentration across the bed due to increased MTH reaction rates at higher inlet concentrations. As a result, the fraction of the catalyst bed that experiences low concentrations of methanol increases, thus lowering the productivity of formaldehyde (vide infra).[32] The increase of selectivities to arene cycle products at higher inlet methanol concentration (e.g., ethene from 3 to 8% and 2MB from 2 to 5%) indicates the promoted arene cycle, which implies inherently higher formaldehyde productivity.[31] The relative sensitivity of the CT_0 to formaldehyde cofeed measured by m_{CT_0} parameter is relatively steady in the low and medium concentration range and displays a substantial decrease at the highest methanol concentration (Figures 3d and S10). On the other side, the relative sensitivity of ethene selectivity to formaldehyde cofeed measured by parameter $m_{C_2H_4}$ decreases monotonically with methanol concentration (Figures 3d and S10). The low values of both m_{CT_0} and $m_{C_2H_4}$ parameters at the highest methanol concentration suggest the higher inherent productivity of this intermediate (eqs 1 and 2). This behavior is in accordance with the measured kinetics of the MIHT reaction over BAS, which is shown to follow a first-order dependence with respect to methanol concentration (Figure 3b).[37,43,44]

Finally, the formaldehyde evolution profiles demonstrate that formaldehyde evolution is strongly promoted at higher reaction temperatures (Figure 1c). Consistent with this, increasing the reaction temperature from 623 via 673 to 773 K (Figure S11) resulted in a decrease of the CT_0 value from 1405, 610, and 190 $g_{CH_3OH}\ g_{cat}^{-1}$. Also, the methane cumulative selectivity increased substantially (from 0.3 to 2.3%) with rising temperature (Figure S11), indicating increased methanol disproportionation and, hence, formaldehyde evolution. At the same time, the cumulative selectivities of the alkene cycle products increased (e.g., butenes from 11.6 to 16.5%), while that of arene cycle products decreased (e.g., ethene from 11 to 8.7%, and 2MB from 5.9 to 3.8%). This increase reflects the dependence of the arene-cycle products on temperature, which is partly accounted for by the increased cracking rate at higher temperatures, favoring the alkene cycle.[2,8,30]

The $m_{C_2H_4}$ parameter shows the highest value at an intermediate temperature of 673 K (Figures 3d and S12), and almost approaches zero at 723 K, indicating the smallest sensitivity of ethene production at high temperatures. On the other side, the m_{CT_0} parameter displays a very prominent decrease with rising temperature (Figures 3d and S12), which concurs the increase in production of formaldehyde with temperature (Figure 3a).[44] These results provide a hint that enhanced formaldehyde formation and reactivity at a high reaction temperature may significantly contribute to a decrease of its stability. Formaldehyde cofeeding experiments also indicate a strong deactivation potential of formaldehyde at low temperatures, wherein a high m_{CT_0} with respect to $m_{C_2H_4}$ values suggests a higher promotion of coke with respect to the arene chain carriers formation.

3.4. Impact of Formaldehyde on the Mechanism of Coking. To analyze the changes in the nature of the MTH

https://doi.org/10.1021/acscatal.3c04279
ACS Catal. 2024, 14, 463−474

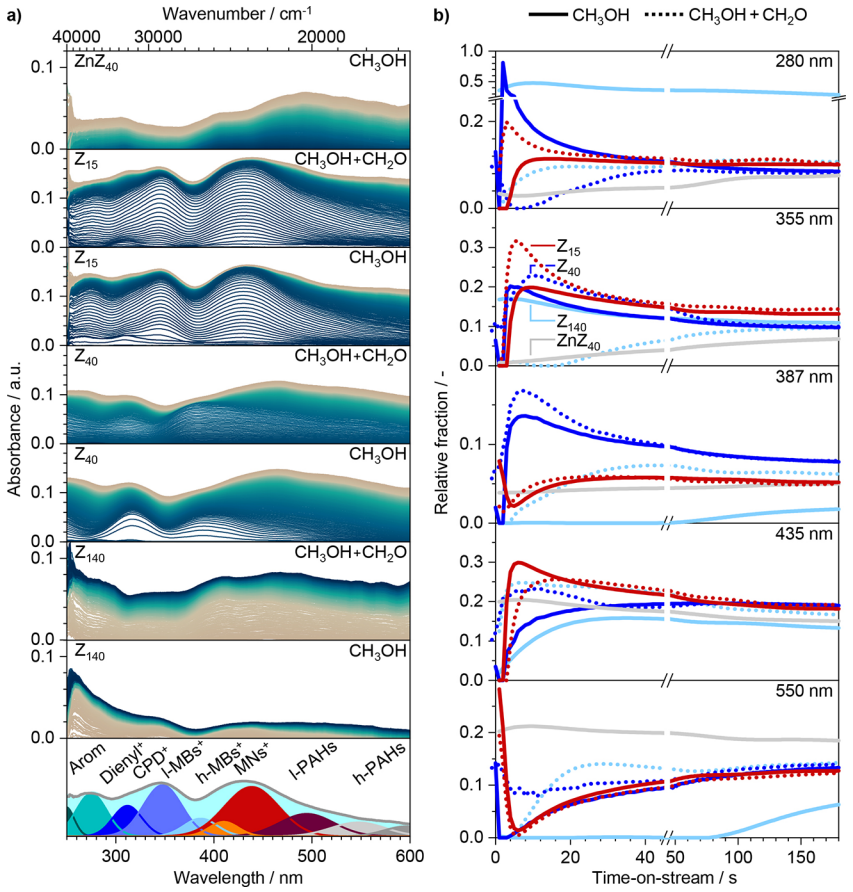

Figure 4. (a) DR-UV/vis spectra of ZSM-5 catalysts during the MTH reaction in the absence and in the presence of formaldehyde cofeeds. (b) Temporal evolution of the relative fractions of specific spectral components obtained by deconvolution into the Gaussian peaks indicated below the spectra in (a). The evolution of all spectral components is presented in Figure S13. Conditions: *WHSV* = 60 (Z_{15}), 41 (Z_{40}, ZnZ_{40}), or 33 (Z_{140}) $g_{CH_3OH}\ g_{cat}^{-1}\ h^{-1}$, c_{CH_3OH} = 11 mol %, c_{CH_2O} = 0 or 2 mol_C %, T = 673 K, and P = 1.2 bar.

intermediates induced by the different inherent formaldehyde productivities over a series of the ZSM-5 catalysts, an operando DR/UV−vis study of the MTH reaction was performed (Figure 4a). This technique provides semiquantitative information on the relative distribution of the active MTH intermediates, such as dienyl(polyenyl), cyclopentadienyl (CPD^+), lower (l-MBs^+), and higher methylated benzenium (h-MBs^+) ions, in parallel to the less active or deactivating species, such as methylated (alkylated) naphthalenes (MNs), and lower (l-PAHs) and higher-molecular-weight PAHs (h-PAHs, Table S3).[51−53] Similar to the catalytic tests performed in a fixed-bed reactor (Figure 2), the DR/UV−vis spectra were recorded over the catalysts operating at incomplete initial conversion (32−85%, Figure S13). In agreement with previous reports and the experimentally measured CT_0 values, the increase in BAS concentration from Z_{140} over Z_{40} to Z_{15} leads to a more prominent formation of h-MBs^+, MNs^+, and PAHs leads to a more prominent formation of h-MBs^+, MNs^+, and PAHs, and reduced relative signals of dienyl, CPD^+, and l-MBs^+ (Figure 4b). This indicates a faster transformation of the latter into the former species. The prevalence of the inactive over the active intermediates is especially pronounced over the ZnZ_{40} catalyst, where the signals of h-MBs^+, MNs^+, and PAHs prevail already in the early stages of the MTH transformation (Figure 4b). The DR/UV−vis results are consistent with the mechanistic hypothesis that the higher productivity of formaldehyde over more acidic and Zn-promoted zeolites may be an important source of the enhanced transformation of active intermediates into coke and consequent deactivation of the catalysts. To further inspect the latter proposal, DR/UV−vis spectra were also recorded in the presence of formaldehyde (2 mol_C %) cofeeds and other conditions unchanged. Similar to the experiments conducted in a fixed-bed reactor, formaldehyde did not bring a change of the initial conversion (Figure S13). Notably, the DR/UV−vis spectral profile of Z_{15} was almost unaffected by the addition of formaldehyde. However, the addition of formaldehyde over Z_{40} and especially Z_{140} catalysts led to much less intense bands associated with active CPD^+ and l-MB^+ intermediates and faster buildup of h-MBs, and deactivating MNs, and PAH species as compared with the experiments performed using pure methanol feed (Figure 4b). In addition, the spectral profile of the low-acidic Z_{140} catalyst recorded upon adding formaldehyde cofeed becomes more similar to those of less stable Z_{15} and ZnZ_{40} materials, which is also consistent with the observed strong decrease of its CT_0 and increase in the selectivity toward the products of the arene HP that are induced by the addition of this intermediate. Overall, the DR/UV−vis spectra evidence that differences in the productivity of formaldehyde over the catalysts have a considerable impact on the transformation of the active HP intermediates into inactive coke species and thus on the catalyst stability in the MTH reaction.

The analysis of a series of Z_{40} catalysts, partially deactivated in the absence or in the presence of the formaldehyde cofeed

https://doi.org/10.1021/acscatal.3c04279
ACS Catal. 2024, 14, 463−474

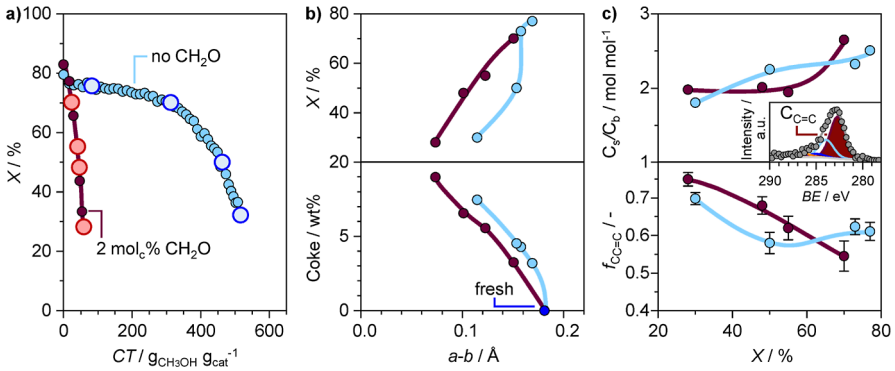

Figure 5. (a) Deactivation profiles of the Z_{40} catalyst during the MTH reaction in the absence and in the presence of formaldehyde cofeed. The points at which partially deactivated catalysts are retrieved for analysis are highlighted. (b) Residual conversion and coke content *versus* $a-b$ parameter difference. (c) The relative ratio of the carbon contents in the outermost surface (probing depth ≈2 nm) and more bulk (probing depth ≥15 nm) regions of the catalysts (C_s/C_b) and the relative fraction of the C_{1s} spectral component associated with C═C bonds in conjugated aromatics such as those in coke *versus* residual conversion. Conditions correspond to those reported in the caption of Figure 2 for the Z_{40} catalyst.

($2\ mol_C$ %), offers additional insights on the impact of formaldehyde on the catalyst propensity to coking (Figure 5a). Except at a low degree of deactivation, the catalysts exposed to the formaldehyde feed exhibit a higher coke content at a similar residual conversion (Figure 5b). Consistent with previous reports,[10] the accumulation of coke resulted in a transformation of the well-resolved reflection doublets at 2θ of 23.5 and 45° in the powder X-ray diffractograms of fresh Z_{40} zeolites into broad single reflections in the respective deactivated catalysts (Figure S14). These changes originate from the contraction of a and elongation of b unit cell parameters owing to lattice strain, induced primarily by the accumulation of coke inside the zeolite micropores. As a result, the difference between a and b parameters constitutes a descriptor that closely reflects the relative content of the internal coke.[10] Although the value of the $a-b$ difference progressively decreases with the extent of zeolite deactivation, the values of this parameter measured at comparable coke contents and similar residual activities are consistently lower when formaldehyde is added to the feed (Figure 5b). These results indicate that formaldehyde promotes the accumulation of coke inside the micropores. Depth profile analysis of coke content by XPS corroborates these findings. More specifically, the catalysts deactivated under formaldehyde cofeed display higher content of carbon both in surface and in subsurface (bulk) region of the catalyst (Figure S15). Still, while the relative ratio of the carbon contents in the surface (probing depth ≈2 nm) and bulk (probing depth ≥15 nm) regions of the catalysts (C_s/C_b) decreased steadily in pure methanol feed, the addition of formaldehyde led to the fast increase of this ratio in the initial stages of deactivation, while its values remained relatively constant during further activity loss (Figure 5c). In addition, for the spectra recorded in the bulk regions of the catalysts, the intensity of the C_{1s} spectral component centered at around 282.6 eV, which is ascribed to C═C bonds in conjugated aromatics like those in coke (Figure 5c, inset), displays an almost linear increase upon catalyst deactivation in the presence of formaldehyde (Figure 5c). In contrast, the fraction of this component in the spectra measured at similar probing depths for the catalyst exposed to pure methanol feed is mostly constant during deactivation, and shows a prominent increase only in the last deactivation stage. The XPS data thus indicate that formaldehyde promotes the formation of aromatic coke species (e.g., PAHs), both on the surface and in the bulk regions of the catalysts, which is in good agreement with the DR/UV−vis analysis. Consistent with the results obtained by the $a-b$ parameter analysis, the C_s/C_b profiles suggest that the addition of formaldehyde leads to a more prominent micropore filling. This mechanism of the micropore filling is different than that displayed by the Z_{40} catalyst under pure methanol feed, wherein most micropores are filled in the late deactivation phase after the slow formation of external coke deposits (Figure 5c). The former may arise from fast buildup of surface coke species, as supported with faster growth of higher PAHs in the DR/UV−vis spectra that are typically proposed to deposit over the external surface of the crystal. Besides, the FMRs may also promote the formation of coke inside the microspores. The more prominent micropore filling with coke is additionally supported by the examination of Z_{15} and Z_{140} catalysts deactivated to a similar level of residual conversion. The values of the $a-b$ parameters for the catalysts deactivated in pure methanol feed and in the presence of formaldehyde are much more different for Z_{40} and especially Z_{140} than for the Z_{15} material (Figure S16). Overall, these results indicate that formaldehyde not only promotes the cascades yielding coke, it does so to preferentially form the internal, micropore coke.

4. CONCLUSIONS

The analysis of formaldehyde evolution in the early stage of the MTH reaction over a series of unpromoted ZSM-5 catalysts showed that the formation of this intermediate proceeds primarily via MIHT over strong BAS in which methanol or DME are hydrogen acceptors (Scheme 1, pathway indicated in light red). The MIHT involving alkenes as hydrogen acceptors likely prevails at higher conversion levels (Scheme 1, pathway indicated in orange). The extraframework zinc ions introduce methanol dehydrogenation, which is a significantly more effective pathway of formaldehyde formation (Scheme 1, pathway indicated in purple). The strong negative correlation between the CT_0 values and STY_{CH_2O} that holds over both unprompted and zinc-promoted zeolites suggests the strong promoting effect of FMRs on coke formation. This is corroborated by the increase in selectivity to the products of the arene cycle and a decrease of the CT_0 values in the presence of the formaldehyde cofeeds, which are much more pronounced for the more stable, low-BAS concentration zeolites than for the less stable, high-BAS concentration and

https://doi.org/10.1021/acscatal.3c04279
ACS Catal. 2024, 14, 463−474

Scheme 1. Formaldehyde Formation Pathways and Its Impact on the Conversion of Alkene into Arene Chain Carriers and Subsequent Transformation of the Latter into Coke as a Function of Catalyst Properties[a]

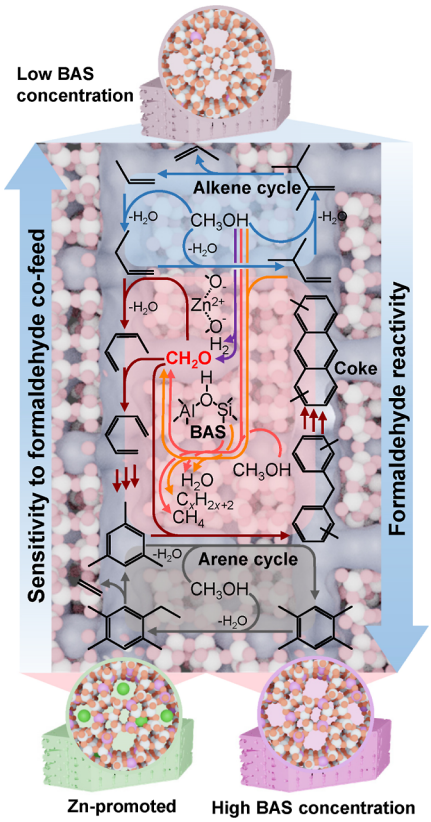

[a]The colors of the arrows indicate specific transformations occurring within the alkene cycle (blue), the arene cycle (gray), MIHT involving methanol or DME (light red), or alkenes (orange) as hydrogen acceptors, methanol dehydrogenation (purple), and FMRs (dark red).

zinc-promoted systems. The evolution of formaldehyde occurs in the first sections of the MTH catalyst bed (ca. $X \leq 30\%$) and is promoted by increasing the methanol concentration and reaction temperature, which are the conditions accelerating catalyst coking. Formaldehyde promotes the transformation of active CPD^+ and MBs^+ into inactive or deactivating MNs and PAH species (Scheme 1, pathways indicated in dark red). As a result, it increases the content of coke at similar residual activities and leads to enhanced micropore coking. Overall, we demonstrate that FMRs have a strong impact on the product distribution and catalyst lifetime in MTH processes.

■ ASSOCIATED CONTENT

Supporting Information

The Supporting Information is available free of charge at https://pubs.acs.org/doi/10.1021/acscatal.3c04279.

Experimental information and discussion, FTIR pyridine adsorption spectra, deactivation profiles, selectivities to hydrocarbon products, cumulative turnover, cumulative selectivity sensitivity factors, additional PEPICO spectra, X-ray diffractograms, and photoemission spectra of the representative catalysts (PDF)

■ AUTHOR INFORMATION

Corresponding Authors

Jeroen A. van Bokhoven − *Institute for Chemical and Bioengineering, ETH Zurich, 8093 Zurich, Switzerland; Paul Scherrer Institute, 5232 Villigen PSI, Switzerland;* orcid.org/0000-0002-4166-2284; Email: jeroen.vanbokhoven@chem.ethz.ch

Vladimir Paunović − *Institute for Chemical and Bioengineering, ETH Zurich, 8093 Zurich, Switzerland;* orcid.org/0000-0001-6630-1672; Email: vladimir.paunovic@chem.ethz.ch

Authors

Charles W. P. Pare − *Institute for Chemical and Bioengineering, ETH Zurich, 8093 Zurich, Switzerland*

Przemyslaw Rzepka − *Institute for Chemical and Bioengineering, ETH Zurich, 8093 Zurich, Switzerland; Paul Scherrer Institute, 5232 Villigen PSI, Switzerland;* orcid.org/0000-0003-3185-3535

Patrick Hemberger − *Paul Scherrer Institute, 5232 Villigen PSI, Switzerland;* orcid.org/0000-0002-1251-4549

Andras Bodi − *Paul Scherrer Institute, 5232 Villigen PSI, Switzerland;* orcid.org/0000-0003-2742-1051

Roland Hauert − *Swiss Federal Laboratories for Materials Science and Technology, Empa, 8600 Dübendorf, Switzerland*

Complete contact information is available at: https://pubs.acs.org/10.1021/acscatal.3c04279

Author Contributions

C.W.P.P. performed the catalytic, N_2 sorption, FTIR, and TGA experiments and analyzed the data. P.R. conducted the XRD analysis. P.H. and A.B. supported the execution of the PEPICO experiments, analysis of the obtained spectra, and discussed the PEPICO data. J.A.v.B. acquired funding and discussed the data. V.P. conceived the idea, performed the PEPICO and UV−vis experiments, analyzed the data, and coordinated this project. V.P. wrote the manuscript with comments and corrections from all the authors.

Notes

The authors declare no competing financial interest.

■ ACKNOWLEDGMENTS

We acknowledge the VUV beamline of the Swiss Light Source at Paul Scherrer Institute (PSI), Villigen, Switzerland for granting a beamtime. Dr. Davide Ferri and Luca Maggiulli from Paul Scherrer Institute are greatly acknowledged for providing the access to the DR/UV−vis cell and spectrometer and for their help in setting up the operando DR/UV−vis experiments. The Energy System Integration platform of the Paul Scherrer Institute is acknowledged for financial support.

■ REFERENCES

(1) Olsbye, U.; Svelle, S.; Bjørgen, M.; Beato, P.; Janssens, T. V. W.; Joensen, F.; Bordiga, S.; Lillerud, K. P. Conversion of Methanol to Hydrocarbons: How Zeolite Cavity and Pore Size Controls Product Selectivity. *Angew. Chem., Int. Ed.* **2012**, *51*, 5810−5831.

(2) Yarulina, I.; Chowdhury, A. D.; Meirer, F.; Weckhuysen, B. M.; Gascon, J. Recent Trends and Fundamental Insights in the Methanol-to-Hydrocarbons Process. *Nat. Catal.* **2018**, *1*, 398−411.

(3) Tian, P.; Wei, Y.; Ye, M.; Liu, Z. Methanol to Olefins (MTO): From Fundamentals to Commercialization. *ACS Catal.* **2015**, *5*, 1922−1938.

(4) Olsbye, U.; Svelle, S.; Lillerud, K. P.; Wei, Z. H.; Chen, Y. Y.; Li, J. F.; Wang, J. G.; Fan, W. B. The Formation and Degradation of Active Species during Methanol Conversion over Protonated Zeotype Catalysts. *Chem. Soc. Rev.* **2015**, *44*, 7155−7176.
(5) Ilias, S.; Bhan, A. Mechanism of the Catalytic Conversion of Methanol to Hydrocarbons. *ACS Catal.* **2013**, *3*, 18−31.
(6) Müller, S.; Liu, Y.; Kirchberger, F. M.; Tonigold, M.; Sanchez-Sanchez, M.; Lercher, J. A. Hydrogen Transfer Pathways during Zeolite Catalyzed Methanol Conversion to Hydrocarbons. *J. Am. Chem. Soc.* **2016**, *138*, 15994−16003.
(7) Bleken, F. L.; Barbera, K.; Bonino, F.; Olsbye, U.; Lillerud, K. P.; Bordiga, S.; Beato, P.; Janssens, T. V. W.; Svelle, S. Catalyst Deactivation by Coke Formation in Microporous and Desilicated Zeolite H-ZSM-5 during the Conversion of Methanol to Hydrocarbons. *J. Catal.* **2013**, *307*, 62−73.
(8) Müller, S.; Liu, Y.; Vishnuvarthan, M.; Sun, X.; van Veen, A. C.; Haller, G. L.; Sanchez-Sanchez, M.; Lercher, J. A. Coke Formation and Deactivation Pathways on H-ZSM-5 in the Conversion of Methanol to Olefins. *J. Catal.* **2015**, *325*, 48−59.
(9) Martinez-Espin, J. S.; Mortén, M.; Janssens, T. V. W.; Svelle, S.; Beato, P.; Olsbye, U. New Insights into Catalyst Deactivation and Product Distribution of Zeolites in the Methanol-to-Hydrocarbons (MTH) Reaction with Methanol and Dimethyl Ether Feeds. *Catal. Sci. Technol.* **2017**, *7*, 2700−2716.
(10) Rojo-Gama, D.; Nielsen, M.; Wragg, D. S.; Dyballa, M.; Holzinger, J.; Falsig, H.; Lundegaard, L. F.; Beato, P.; Brogaard, R. Y.; Lillerud, K. P.; Olsbye, U.; Svelle, S. A Straightforward Descriptor for the Deactivation of Zeolite Catalyst H-ZSM-5. *ACS Catal.* **2017**, *7*, 8235−8246.
(11) Foley, B. L.; Johnson, B. A.; Bhan, A. Kinetic Evaluation of Deactivation Pathways in Methanol-to-Hydrocarbon Catalysis on HZSM-5 with Formaldehyde, Olefinic, Dieneic, and Aromatic Co-Feeds. *ACS Catal.* **2021**, *11*, 3628−3637.
(12) Valecillos, J.; Vicente, H.; Gayubo, A. G.; Aguayo, A. T.; Castaño, P. Spectro-Kinetics of the Methanol to Hydrocarbons Reaction Combining Online Product Analysis with UV-Vis and FTIR Spectroscopies throughout the Space Time Evolution. *J. Catal.* **2022**, *408*, 115−127.
(13) Hwang, A.; Bhan, A. Deactivation of Zeolites and Zeotypes in Methanol-to-Hydrocarbons Catalysis: Mechanisms and Circumvention. *Acc. Chem. Res.* **2019**, *52*, 2647−2656.
(14) Lee, S.; Choi, M. Unveiling Coke Formation Mechanism in MFI Zeolites during Methanol-to-Hydrocarbons Conversion. *J. Catal.* **2019**, *375*, 183−192.
(15) Barbera, K.; Sørensen, S.; Bordiga, S.; Skibsted, J.; Fordsmand, H.; Beato, P.; Janssens, T. V. W. Role of Internal Coke for Deactivation of ZSM-5 Catalysts after Low Temperature Removal of Coke with NO_2. *Catal. Sci. Technol.* **2012**, *2*, 1196.
(16) Wei, Y.; Yuan, C.; Li, J.; Xu, S.; Zhou, Y.; Chen, J.; Wang, Q.; Xu, L.; Qi, Y.; Zhang, Q.; Liu, Z. Coke Formation and Carbon Atom Economy of Methanol-to-Olefins Reaction. *ChemSusChem* **2012**, *5* (5), 906−912.
(17) Campbell, S. M.; Bibby, D. M.; Coddington, J. M.; Howe, R. F. Dealumination of HZSM-5 Zeolites. *J. Catal.* **1996**, *161*, 350−358.
(18) Schmidt, F.; Hoffmann, C.; Giordanino, F.; Bordiga, S.; Simon, P.; Carrillo-Cabrera, W.; Kaskel, S. Coke Location in Microporous and Hierarchical ZSM-5 and the Impact on the MTH Reaction. *J. Catal.* **2013**, *307*, 238−245.
(19) Paunović, V.; Sushkevich, V.; Rzepka, P.; Artiglia, L.; Hauert, R.; Sik Lee, S.; van Bokhoven, J. A. Reactivation of Catalysts for Methanol-to-Hydrocarbons Conversion with Hydrogen. *J. Catal.* **2022**, *407*, 54−64.
(20) Zhang, X.; Liu, D.; Xu, D.; Asahina, S.; Cychosz, K. A.; Agrawal, K. V.; Al Wahedi, Y.; Bhan, A.; Al Hashimi, S.; Terasaki, O.; Thommes, M.; Tsapatsis, M. Synthesis of Self-Pillared Zeolite Nanosheets by Repetitive Branching. *Science* **2012**, *336*, 1684−1687.
(21) Almutairi, S. M. T.; Mezari, B.; Pidko, E. A.; Magusin, P. C. M. M.; Hensen, E. J. M. Influence of Steaming on the Acidity and the Methanol Conversion Reaction of HZSM-5 Zeolite. *J. Catal.* **2013**, *307*, 194−203.
(22) Milina, M.; Mitchell, S.; Cooke, D.; Crivelli, P.; Pérez-Ramírez, J. Impact of Pore Connectivity on the Design of Long-Lived Zeolite Catalysts. *Angew. Chem., Int. Ed.* **2015**, *54*, 1591−1594.
(23) Liang, T.; Chen, J.; Qin, Z.; Li, J.; Wang, P.; Wang, S.; Wang, G.; Dong, M.; Fan, W.; Wang, J. Conversion of Methanol to Olefins over H-ZSM-5 Zeolite: Reaction Pathway Is Related to the Framework Aluminum Siting. *ACS Catal.* **2016**, *6*, 7311−7325.
(24) Dai, H.; Shen, Y.; Yang, T.; Lee, C.; Fu, D.; Agarwal, A.; Le, T. T.; Tsapatsis, M.; Palmer, J. C.; Weckhuysen, B. M.; Dauenhauer, P. J.; Zou, X.; Rimer, J. D. Finned Zeolite Catalysts. *Nat. Mater.* **2020**, *19*, 1074−1080.
(25) Yarulina, I.; De Wispelaere, K.; Bailleul, S.; Goetze, J.; Radersma, M.; Abou-Hamad, E.; Vollmer, I.; Goesten, M.; Mezari, B.; Hensen, E. J. M.; Martínez-Espín, J. S.; Morten, M.; Mitchell, S.; Perez-Ramirez, J.; Olsbye, U.; Weckhuysen, B. M.; Van Speybroeck, V.; Kapteijn, F.; Gascon, J. Structure-Performance Descriptors and the Role of Lewis Acidity in the Methanol-to-Propylene Process. *Nat. Chem.* **2018**, *10*, 804−812.
(26) Pinilla-Herrero, I.; Borfecchia, E.; Holzinger, J.; Mentzel, U. V.; Joensen, F.; Lomachenko, K. A.; Bordiga, S.; Lamberti, C.; Berlier, G.; Olsbye, U.; Svelle, S.; Skibsted, J.; Beato, P. High Zn/Al Ratios Enhance Dehydrogenation vs Hydrogen Transfer Reactions of Zn-ZSM-5 Catalytic Systems in Methanol Conversion to Aromatics. *J. Catal.* **2018**, *362*, 146−163.
(27) Fu, T.; Shao, J.; Li, Z. Catalytic Synergy between the Low Si/Al Ratio Zn/ZSM-5 and High Si/Al Ratio HZSM-5 for High-Performance Methanol Conversion to Aromatics. *Appl. Catal., B* **2021**, *291*, 120098.
(28) Ni, Y.; Zhu, W.; Liu, Z. Formaldehyde Intermediate Participating in the Conversion of Methanol to Aromatics over Zinc Modified H-ZSM-5. *J. Energy Chem.* **2021**, *54*, 174−178.
(29) Yarulina, I.; Bailleul, S.; Pustovarenko, A.; Martinez, J. R.; Wispelaere, K. D.; Hajek, J.; Weckhuysen, B. M.; Houben, K.; Baldus, M.; Van Speybroeck, V.; Kapteijn, F.; Gascon, J. Suppression of the Aromatic Cycle in Methanol-to-Olefins Reaction over ZSM-5 by Post-Synthetic Modification Using Calcium. *ChemCatChem* **2016**, *8*, 3057−3063.
(30) Kim, H.; Jang, H. G.; Jang, E.; Park, S. J.; Lee, T.; Jeong, Y.; Baik, H.; Cho, S. J.; Choi, J. On Methanol to Hydrocarbons Reactions in a Hierarchically Structured ZSM-5 Zeolite Catalyst. *Catal. Today* **2018**, *303*, 150−158.
(31) Arora, S. S.; Bhan, A. The Critical Role of Methanol Pressure in Controlling Its Transfer Dehydrogenation and the Corresponding Effect on Propylene-to-Ethylene Ratio during Methanol-to-Hydrocarbons Catalysis on H-ZSM-5. *J. Catal.* **2017**, *356*, 300−306.
(32) Hwang, A.; Kumar, M.; Rimer, J. D.; Bhan, A. Implications of Methanol Disproportionation on Catalyst Lifetime for Methanol-to-Olefins Conversion by HSSZ-13. *J. Catal.* **2017**, *346*, 154−160.
(33) Foley, B. L.; Johnson, B. A.; Bhan, A. A Method for Assessing Catalyst Deactivation: A Case Study on Methanol-to-Hydrocarbons Conversion. *ACS Catal.* **2019**, *9*, 7065−7072.
(34) Wu, X.; Xu, S.; Wei, Y.; Zhang, W.; Huang, J.; Xu, S.; He, Y.; Lin, S.; Sun, T.; Liu, Z. Evolution of C-C Bond Formation in the Methanol-to-Olefins Process: From Direct Coupling to Autocatalysis. *ACS Catal.* **2018**, *8* (8), 7356−7361.
(35) Arora, S. S.; Shi, Z.; Bhan, A. Mechanistic Basis for Effects of High-Pressure H2 Cofeeds on Methanol-to-Hydrocarbons Catalysis over Zeolites. *ACS Catal.* **2019**, *9*, 6407−6414.
(36) Hwang, A.; Bhan, A. Bifunctional Strategy Coupling Y 2 O 3 -Catalyzed Alkanal Decomposition with Methanol-to-Olefins Catalysis for Enhanced Lifetime. *ACS Catal.* **2017**, *7* (7), 4417−4422.
(37) Arora, S. S.; Nieskens, D. L. S.; Malek, A.; Bhan, A. Lifetime Improvement in Methanol-to-Olefins Catalysis over Chabazite Materials by High-Pressure H2 Co-Feeds. *Nat. Catal.* **2018**, *1*, 666−672.
(38) Liu, Y.; Kirchberger, F. M.; Müller, S.; Eder, M.; Tonigold, M.; Sanchez-Sanchez, M.; Lercher, J. A. Critical Role of Formaldehyde

https://doi.org/10.1021/acscatal.3c04279
ACS Catal. 2024, 14, 463−474

during Methanol Conversion to Hydrocarbons. *Nat. Commun.* **2019**, *10*, 1462.
(39) Wen, W.; Yu, S.; Zhou, C.; Ma, H.; Zhou, Z.; Cao, C.; Yang, J.; Xu, M.; Qi, F.; Zhang, G.; Pan, Y. Formation and Fate of Formaldehyde in Methanol-to-Hydrocarbon Reaction: In Situ Synchrotron Radiation Photoionization Mass Spectrometry Study. *Angew. Chem., Int. Ed.* **2020**, *59*, 4873−4878.
(40) Liu, Y.; Müller, S.; Berger, D.; Jelic, J.; Reuter, K.; Tonigold, M.; Sanchez-Sanchez, M.; Lercher, J. A. Formation Mechanism of the First Carbon-Carbon Bond and the First Olefin in the Methanol Conversion into Hydrocarbons. *Angew. Chem., Int. Ed.* **2016**, *55*, 5723−5726.
(41) Martinez-Espin, J. S.; De Wispelaere, K.; Westgård Erichsen, M.; Svelle, S.; Janssens, T. V. W.; Van Speybroeck, V.; Beato, P.; Olsbye, U. Benzene Co-Reaction with Methanol and Dimethyl Ether over Zeolite and Zeotype Catalysts: Evidence of Parallel Reaction Paths to Toluene and Diphenylmethane. *J. Catal.* **2017**, *349*, 136−148.
(42) Sun, X.; Mueller, S.; Liu, Y.; Shi, H.; Haller, G. L.; Sanchez-Sanchez, M.; Van Veen, A. C.; Lercher, J. A. On Reaction Pathways in the Conversion of Methanol to Hydrocarbons on HZSM-5. *J. Catal.* **2014**, *317*, 185−197.
(43) Kilburn, L.; DeLuca, M.; Hoffman, A. J.; Patel, S.; Hibbitts, D. Comparing Alkene-Mediated and Formaldehyde-Mediated Diene Formation Routes in Methanol-to-Olefins Catalysis in MFI and CHA. *J. Catal.* **2021**, *400*, 124−139.
(44) Kirchberger, F. M.; Liu, Y.; Plessow, P. N.; Tonigold, M.; Studt, F.; Sanchez-Sanchez, M.; Lercher, J. A. Mechanistic Differences between Methanol and Dimethyl Ether in Zeolite-Catalyzed Hydrocarbon Synthesis. *Proc. Natl. Acad. Sci. U.S.A.* **2022**, *119*, No. e2103840119.
(45) Lin, S.; Zhi, Y.; Zhang, W.; Yuan, X.; Zhang, C.; Ye, M.; Xu, S.; Wei, Y.; Liu, Z. Hydrogen Transfer Reaction Contributes to the Dynamic Evolution of Zeolite-Catalyzed Methanol and Dimethyl Ether Conversions: Insight into Formaldehyde. *Chin. J. Catal.* **2023**, *46*, 11−27.
(46) Martínez-Espín, J. S.; De Wispelaere, K.; Janssens, T. V. W.; Svelle, S.; Lillerud, K. P.; Beato, P.; Van Speybroeck, V.; Olsbye, U. Hydrogen Transfer versus Methylation: On the Genesis of Aromatics Formation in the Methanol-To-Hydrocarbons Reaction over H-ZSM-5. *ACS Catal.* **2017**, *7*, 5773−5780.
(47) Paunović, V.; Hemberger, P.; Bodi, A.; Hauert, R.; van Bokhoven, J. A. Impact of Nonzeolite-Catalyzed Formation of Formaldehyde on the Methanol-to-Hydrocarbons Conversion. *ACS Catal.* **2022**, *12*, 13426−13434.
(48) Wei, Z.; Chen, Y. Y.; Li, J.; Guo, W.; Wang, S.; Dong, M.; Qin, Z.; Wang, J.; Jiao, H.; Fan, W. Stability and Reactivity of Intermediates of Methanol Related Reactions and C-C Bond Formation over H-ZSM-5 Acidic Catalyst: A Computational Analysis. *J. Phys. Chem. C* **2016**, *120*, 6075−6087.
(49) Ni, Y.; Zhu, W.; Liu, Z. H-ZSM-5-Catalyzed Hydroacylation Involved in the Coupling of Methanol and Formaldehyde to Aromatics. *ACS Catal.* **2019**, *9*, 11398−11403.
(50) Hemberger, P.; Van Bokhoven, J. A.; Pérez-Ramírez, J.; Bodi, A. New Analytical Tools for Advanced Mechanistic Studies in Catalysis: Photoionization and Photoelectron Photoion Coincidence Spectroscopy. *Catal. Sci. Technol.* **2020**, *10*, 1975−1990.
(51) Mores, D.; Stavitski, E.; Kox, M. H. F.; Kornatowski, J.; Olsbye, U.; Weckhuysen, B. M. Space- And Time-Resolved in-Situ Spectroscopy on the Coke Formation in Molecular Sieves: Methanol-to-Olefin Conversion over H-ZSM-5 and H-SAPO-34. *Chem.—Eur. J.* **2008**, *14*, 11320−11327.
(52) Goetze, J.; Meirer, F.; Yarulina, I.; Gascon, J.; Kapteijn, F.; Ruiz-Martínez, J.; Weckhuysen, B. M. Insights into the Activity and Deactivation of the Methanol-to-Olefins Process over Different Small-Pore Zeolites As Studied with Operando UV-Vis Spectroscopy. *ACS Catal.* **2017**, *7*, 4033−4046.
(53) Fu, D.; van der Heijden, O.; Stanciakova, K.; Schmidt, J. E.; Weckhuysen, B. M. Disentangling Reaction Processes of Zeolites within Single-Oriented Channels. *Angew. Chem., Int. Ed.* **2020**, *59*, 15502−15506.
(54) Sztáray, B.; Voronova, K.; Torma, K. G.; Covert, K. J.; Bodi, A.; Hemberger, P.; Gerber, T.; Osborn, D. L. CRF-PEPICO: Double Velocity Map Imaging Photoelectron Photoion Coincidence Spectroscopy for Reaction Kinetics Studies. *J. Chem. Phys.* **2017**, *147* (1), 013944.
(55) Bodi, A.; Sztáray, B.; Baer, T.; Johnson, M.; Gerber, T. Data Acquisition Schemes for Continuous Two-Particle Time-of-Flight Coincidence Experiments. *Rev. Sci. Instrum.* **2007**, *78*, 084102.
(56) Osborn, D. L.; Hayden, C. C.; Hemberger, P.; Bodi, A.; Voronova, K.; Sztáray, B. Breaking through the False Coincidence Barrier in Electron - Ion Coincidence Experiments. *J. Chem. Phys.* **2016**, *145*, 164202.
(57) Bodi, A.; Johnson, M.; Gerber, T.; Gengeliczki, Z.; Sztáray, B.; Baer, T. Imaging Photoelectron Photoion Coincidence Spectroscopy with Velocity Focusing Electron Optics. *Rev. Sci. Instrum.* **2009**, *80*, 034101.
(58) Janssens, T. V. W.; Svelle, S.; Olsbye, U. Kinetic Modeling of Deactivation Profiles in the Methanol-to-Hydrocarbons (MTH) Reaction: A Combined Autocatalytic-Hydrocarbon Pool Approach. *J. Catal.* **2013**, *308*, 122−130.

https://doi.org/10.1021/acscatal.3c04279
ACS Catal. 2024, 14, 463−474